

# Chiral and Continuum Extrapolation of Partially-Quenched Lattice Results

C. R. Allton,<sup>1</sup> W. Armour,<sup>1</sup> D. B. Leinweber,<sup>2</sup> A. W. Thomas,<sup>3</sup> and R. D. Young<sup>3</sup>

<sup>1</sup>*Department of Physics, University of Wales Swansea, Swansea SA2 8PP, Wales, U.K.*

<sup>2</sup>*CSSM and Department of Physics, University of Adelaide, Adelaide SA 5005, Australia*

<sup>3</sup>*Jefferson Lab, 12000 Jefferson Ave., Newport News VA 23606, USA*

The vector meson mass is extracted from a large sample of partially quenched, two-flavor lattice QCD simulations. For the first time, discretisation, finite-volume and partial quenching artefacts are treated in a unified chiral effective field theory analysis of the lattice simulation results.

Recent developments in lattice QCD have enabled the first large-scale simulation of chiral, dynamical fermions [1]. While this accomplishment is a significant milestone in the progress towards an accurate description of physical QCD, the high demand on computing resources restricts practical calculations to an unphysical domain of simulation parameters. In particular, lattice QCD involves a discretised space-time of finite spatial extent, with input quark masses much larger than those in Nature. Each of these approximations requires special attention in the extraction of physical observables from Monte Carlo simulations. In this Letter we analyse a very large set of partially quenched data for the mass of the  $\rho$  meson. We show that a systematic analysis of this data within finite range regularised effective field theory enables us to remove the effects of partial quenching and to take both the continuum and infinite volume limits. The resulting data lies on a single, well defined curve which extrapolates to a value within 1% of the physical  $\rho$  mass. The contrast between the raw lattice data (note the scatter in Fig. 2) and the corrected data shown in Fig. 3 is striking.

Spontaneous chiral symmetry breaking in QCD dictates that, in the vicinity of the chiral limit, hadronic observables exhibit nonanalytic dependence on the quark mass [2]. This feature places tight constraints on the form of chiral extrapolations if they are to be consistent with the properties of low-energy QCD [3, 4]. The most natural solution to this problem is to use effective field theory (EFT) to describe the quark-mass dependence of hadron properties. Considering a benchmark quantity, such as the nucleon mass, there is substantial phenomenological information on the quark-mass expansion near the chiral limit [5]. In the context of lattice simulations, where quark masses are significantly far from the chiral limit, the expansion is acutely sensitive to higher-order corrections. Fortunately, such issues can be alleviated by reformulating the EFT in the framework of finite-range regularisation (FRR) [6] — with demonstrated success in the efficient extrapolation [7] of lattice calculations of the nucleon mass [8].

Provided simulations are performed on a suitably large *box*, finite-volume corrections will be exponentially suppressed. Nevertheless, these leading corrections can be described by the same low-energy effective field theory

used to understand the quark-mass variation [9]. Finite-volume corrections are dominated by the suppression of the infrared component of chiral loop diagrams — as observed in a recent study of volume dependence in lattice QCD [10]. Corrections of this type have previously been incorporated in quark-mass extrapolations [11, 12, 13]. They are essential in the case of the  $p$ -wave decay channels, such as  $\rho \rightarrow \pi\pi$  [11] and  $\Delta \rightarrow N\pi$  [12]. The modifications to EFT on a finite volume have been investigated for a range of observables — e.g., see Refs. [14, 15, 16, 17].

Removal of discretisation artefacts from simulation results also represents an important step in the systematic extraction of continuum QCD physics. From a technical point of view, a great deal of effort has gone into action improvement [18] such that near-continuum results can be obtained at finite lattice spacing [19, 20, 21]. Residual discrepancies from the continuum can be incorporated as perturbative corrections in EFT [22, 23, 24, 25], thereby providing a systematic approach to the continuum.

The generation of gauge field configurations with dynamical sea quarks is the most computationally demanding component of the calculation of standard observables. By comparison, the matrix inversion required to obtain quark propagators is relatively efficient. This enables the calculation of quark propagators over a range of quark masses for a fixed gauge field ensemble. Such calculations are referred to as partially quenched QCD (pQQCD), where the valence quark masses no longer match those simulated in the sea. Although an unphysical approximation, the connection to the physical theory in EFT has been demonstrated [26]. Most importantly, the partially quenched EFT does not require any new, unphysical parameters.

Effective field theory therefore provides a consolidated framework for the analysis of the dependence of hadronic observables on sea and valence quark masses, as well as lattice volume and spacing. In this Letter we present a global analysis of a very large set of sophisticated lattice simulation results. The aim is to produce an accurate determination of the (real part of the)  $\rho$ -meson mass in 2-flavour QCD, with the required input of the experimental width. For a complete account of the analysis procedure, the reader is referred to Ref. [27].

Partially-quenched lattice simulations are characterised by the distinction between the masses of quarks

coupling to external sources and those associated with vacuum polarisation of the gauge field. Subsequently, the construction of effective field theories based on such simulations necessarily distinguishes the *valence*- and *sea*-quark composition of hadronic states. While the external legs of any  $n$ -point hadronic correlator are constructed of valence quarks only, internal (hadron) loop diagrams may comprise any mixture of sea and valence quarks. The mass of a particular vector meson state is therefore described by

$$M_{ijk}^a = M(a, m_i; m_j, m_k), \quad (1)$$

where the first two parameters of  $M(a, m_i; m_j, m_k)$  specify the gauge field ensemble with lattice spacing  $a$  and sea-quark mass  $m_{\text{sea}} = m_i$ . The masses of the valence quarks are given by  $m_j$  and  $m_k$ . Similarly,  $m_{ijk}^a$  is the mass of a pseudoscalar meson of equivalent quark composition.

The global parameterisation of the vector meson mass, dependent on quark masses, lattice spacing and physical volume, is written as

$$M_{ijj}^{a\ 2} = (\alpha_0 + X_2 a^2 + \alpha_2 m_{ijj}^{a\ 2} + \alpha_4 m_{ijj}^{a\ 4})^2 + \Sigma_{a;ijj}^{\text{TOT}}(L). \quad (2)$$

The total loop correction to the  $M_{ijj}^a$  meson, on a finite box of physical length  $L = Na$ , is described by

$$\Sigma_{a;ijj}^{\text{TOT}}(L) = \Sigma_{\pi\pi}^\rho(m_{ijj}^a, L) + \Sigma_{\pi\omega}^\rho(m_{ijj}^a, L) + \Sigma_{\eta'\rho}^\rho(m_{ijj}^a, m_{ijj}^a, m_{iii}^a, L). \quad (3)$$

The relevant loop corrections are depicted in Fig. 1. The corresponding loop integrals, in the  $L \rightarrow \infty$  limit, are given by

$$\Sigma_{\pi\pi}^\rho(m_{ijj}^a) = -\frac{f_{\rho\pi\pi}^2}{24\pi^3} \int d^3k \frac{k^2 u_{\pi\pi}^2(k)}{\sqrt{k^2 + m_{ijj}^{a\ 2}} [k^2 + m_{ijj}^{a\ 2} - \mu_\rho^2/4]}, \quad (4)$$

$$\Sigma_{\pi\omega}^\rho(m_{ijj}^a) = -\frac{\mu_\rho g_2^2}{12\pi^3 f_\pi^2} \int d^3k \frac{k^2 u^2(k)}{\sqrt{k^2 + m_{ijj}^{a\ 2}} \left[ \sqrt{k^2 + m_{ijj}^{a\ 2}} + (M_{ijj}^a - M_{ijj}^a) \right]}, \quad (5)$$

$$\Sigma_{\eta'\rho}^\rho(m_{ijj}^a, m_{ijj}^a, m_{iii}^a) = \frac{\mu_\rho g_2^2}{12\pi^3 f_\pi^2} \int d^3k \frac{k^2 u^2(k)}{(k^2 + m_{ijj}^{a\ 2})} \left\{ \frac{(m_{ijj}^{a\ 2} - m_{ijj}^{a\ 2})}{(k^2 + m_{ijj}^{a\ 2})} + \frac{(m_{iii}^{a\ 2} - m_{ijj}^{a\ 2})}{(k^2 + m_{ijj}^{a\ 2})} \right\}. \quad (6)$$

Symbols are summarised as:  $f_\pi = 93 \text{ MeV}$ ; physical  $\rho$  and  $\pi$  masses,  $\mu_\rho = 0.770 \text{ GeV}$  and  $\mu_\pi = 0.140 \text{ GeV}$ ;  $\rho\pi\pi$  coupling  $f_{\rho\pi\pi} = 6.028$  [11];  $g_2$  (as introduced in Ref. [28]) is related to the  $\omega\rho\pi$  coupling,  $g_{\omega\rho\pi} = 16 \text{ GeV}^{-1}$  [29], by  $g_2 = g_{\omega\rho\pi} f_\pi / 2 = 0.74$ ;  $k = |\vec{k}|$ ; finite-range regularisation is implemented with a dipole form,  $u(k) = (1 + k^2/\Lambda^2)^{-2}$ , and the  $\rho\pi\pi$  coupling is preserved at the physical threshold,  $u_{\pi\pi}(k) = u(k)u^{-1}(\sqrt{\mu_\rho^2/4 - \mu_\pi^2})$ .

The leading finite-volume corrections are trivially incorporated by replacing the continuum loop integrals in Eqs. (4,5,6) by a sum over discrete momenta [11, 12, 13]

$$\int d^3k \rightarrow \left(\frac{2\pi}{L}\right)^3 \sum_{\vec{k}}, \quad (7)$$

where  $\vec{k} = (2\pi/L)\vec{i}$  for  $\vec{i} \in \mathbb{Z}^3$ . This modification produces an infrared suppression of the loop integrals, and

is independent of the choice of ultra-violet regularisation [14].

The bracketed term in Eq. (2) describes the residual variation of the vector meson mass which is not constrained by the low-energy EFT. The analytic variation of the quark-mass dependence is characterised by the continuum parameters,  $\alpha_i$ . At finite lattice spacing, all terms at order  $a$  and  $a^2$  must be treated consistently with the symmetry breaking patterns of the prescribed fermion action [22]. This can potentially lead to more singular chiral behaviour in the effective field theory at finite lattice spacing [24]. In this study, the leading lattice spacing corrections to the terms analytic in the quark mass are investigated.

The lattice simulation data considered in this analysis come from a large sample of partially quenched simulation results from the CP-PACS Collaboration [8]. These

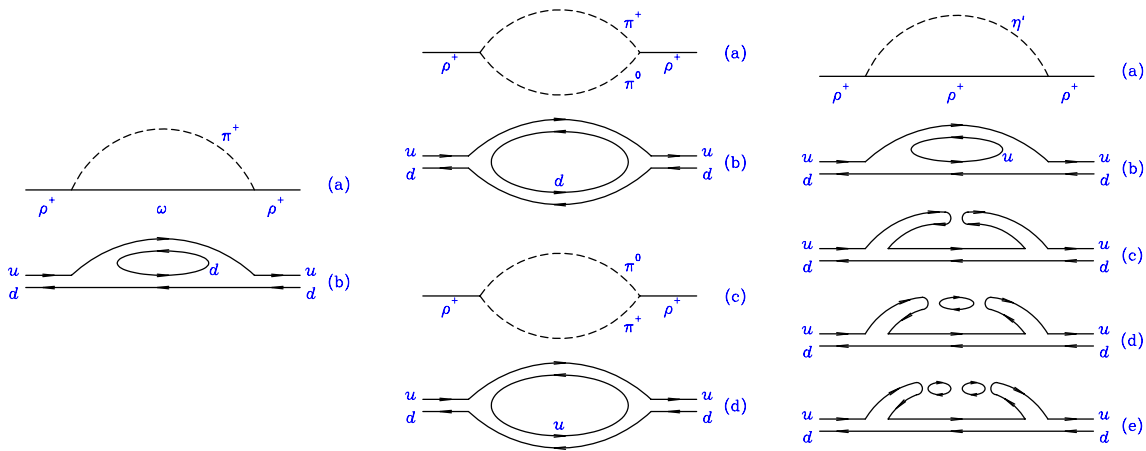


FIG. 1: Left: Diagram providing the leading nonanalytic contribution to the chiral expansion of the  $\rho$ -meson mass (a) and its associated quark-flow (b). Middle: Two-pion contributions, (a), (c), to the  $\rho$ -meson self-energy and their associated quark-flow, (b), (d), respectively. Right: The  $\eta'$  contribution (a) and its associated quark flow diagrams in pQCD. While diagram (c) appears in quenched QCD, in pQCD (or full QCD) it is complemented by an infinite series of terms, the first two of which are depicted in diagrams (d) and (e).

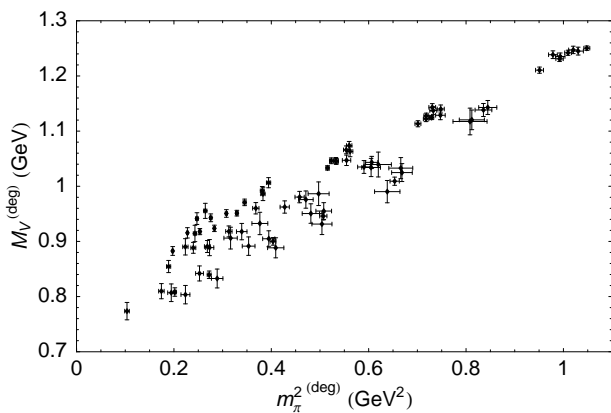


FIG. 2: Partially-quenched vector meson masses plotted versus “degenerate” pion mass squared. Here  $M_V^{(deg)} = M_{ijj}^a$  and  $m_\pi^{(deg)} = m_{ijj}^a$ . The simulation results are from CP-PACS [8].

simulations were performed using mean-field improved clover fermions at four different couplings,  $\beta$ . For each value of the coupling, four different sea quark masses have been calculated, yielding a total of 16 independent gauge field ensembles. On each ensemble, the quark propagator has been evaluated for five values of the valence quark mass. For the vector mesons constructed of degenerate valence quarks there are a total of 80 “data” points. The lattice scale is set via the QCD Sommer scale  $r_0 = 0.49 \text{ fm}$  [30], enabling all of these points to be shown in physical units — as in Fig. 2.

The form provided by Eq. (2) allows a universal fit to all these points with just four free parameters (plus regulator scale). This is therefore a highly constrained fit to the large sample of simulation results. The best fit parameters are displayed in Table I. The  $\chi^2$  indicates

TABLE I: The resulting global fit to the entire sample of lattice results (with  $\Lambda = 660 \text{ MeV}$ ).

$\alpha_0$	$X_2$	$\alpha_2$	$\alpha_4$	$\chi^2/d.o.f.$
(GeV)	(GeV-fm $^{-2}$ )	(GeV $^{-1}$ )	(GeV $^{-3}$ )	
$0.832^{+4}_{-4}$	$-1.40^{+3}_{-4}$	$0.494^{+12}_{-11}$	$-0.061^{+8}_{-9}$	39 / 76

that Eq. (2) accurately describes this large quantity of data. The regulator mass,  $\Lambda$ , has also been optimised to produce a best fit to the data, namely  $\Lambda = 660 \pm 30 \text{ MeV}$ . Studying the variation of the fit over this domain introduces a small additional uncertainty to the extrapolated result which is listed below in the error estimate.

Variations of Eq. (2) have also been investigated. Scaling corrections to the parameters  $\alpha_2$  and  $\alpha_4$  yield coefficients which are consistent with zero. Linear corrections in the lattice spacing, taking the form of a term  $X_1 a$ , are observed to be small and hence do not improve on the fit with  $X_1 = 0$ . Extending to higher analytic order in the quark mass expansion, by a term  $\alpha_6 m_\pi^6$ , reduces the stability of the fit, indicating that the data are consistent with  $\alpha_6 = 0$  — see Ref. [27] for a complete account of these effects. The systematic error quoted below covers the range found with all of these variations.

The fit parameters shown in Table I allow one to shift the simulation results to the infinite-volume, continuum limit and to remove the effects of partial quenching — hence restoring unitarity in the quark masses. Complete details of the procedure are outlined in Ref. [27]. The results are displayed in Fig. 3, where we observe a remarkable result. The tremendous spread of data seen in Fig. 2 is dramatically reduced, with all 80 points now lying very accurately on a universal curve.

The curve through Fig. 3 displays the determined variation of the  $\rho$ -meson mass with pion mass. This curve also presents an extrapolation to the physical point, al-

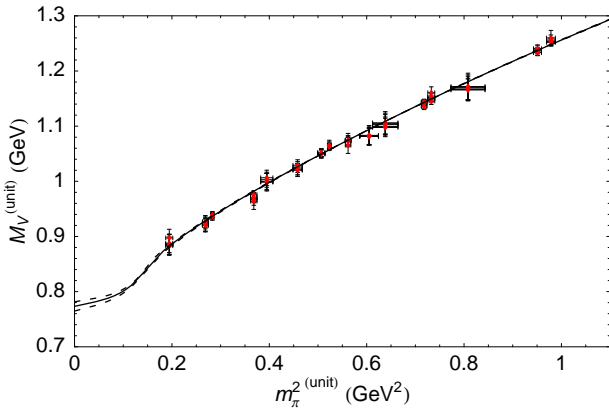


FIG. 3: The same 80 lattice data points as in Fig. 2, after correction to restore the infinite-volume, continuum and quark-mass unitarity limits. The central curve displays the best-fit from the global analysis. The dashed curves show the bounds on the FRR scale,  $0.630 < \Lambda < 0.690$  GeV.

lowing extraction of the physical  $\rho$ -meson mass

$$M_\rho = 777(4)_{-0}^{+13}(8) \text{ MeV}, \quad (8)$$

where the first error is statistical, the second is from variations of the fit procedure and the third from the determination of  $\Lambda$  [27]. This result is in excellent agreement with the experimentally observed mass.

This analysis demonstrates the ability to treat all lattice artifacts within a unified framework. Both scaling violations and finite-volume discrepancies can be removed through the procedure outlined. The number of simulation points can be increased dramatically by including partially quenched results. This in turn permits a highly constrained fit to produce an accurate extrapolation to the physical point. With minimal input, namely the  $\rho\pi\pi$  and  $\omega\rho\pi$  coupling constants, the real part of the  $\rho$ -meson mass has been accurately determined in two-flavour QCD [31]. The final result for the pion mass variation, as described by the universal curve in Fig. 3, sets a benchmark for the continuum, infinite-volume limit of the  $\rho$  meson in two-flavour QCD.

CRA and WA would like to thank the CSSM for their support and kind hospitality. WA would like to thank PPARC for support. The authors would like to thank W. Melnitchouk, D. Richards, G. Shore and S. Wright for helpful comments. This work was supported by the Australian Research Council and by DOE contract DE-AC05-84ER40150, under which SURA operates Jefferson Laboratory.

- [2] L. F. Li and H. Pagels, Phys. Rev. Lett. **26**, 1204 (1971).
- [3] D. B. Leinweber, D. H. Lu and A. W. Thomas, Phys. Rev. D **60**, 034014 (1999) [arXiv:hep-lat/9810005].
- [4] D. B. Leinweber, A. W. Thomas, K. Tsushima and S. V. Wright, Phys. Rev. D **61**, 074502 (2000) [arXiv:hep-lat/9906027].
- [5] B. Borasoy and U. G. Meissner, Annals Phys. **254**, 192 (1997) [arXiv:hep-ph/9607432].
- [6] R. D. Young, D. B. Leinweber and A. W. Thomas, Prog. Part. Nucl. Phys. **50**, 399 (2003)
- [7] D. B. Leinweber, A. W. Thomas and R. D. Young, Phys. Rev. Lett. **92** (2004) 242002
- [8] A. Ali Khan *et al.* [CP-PACS Collaboration], Phys. Rev. D **65**, 054505 (2002) [Erratum-ibid. D **67**, 059901 (2003)]
- [9] J. Gasser and H. Leutwyler, Nucl. Phys. B **307**, 763 (1988).
- [10] A. Ali Khan *et al.* [QCDSF-UKQCD Collaboration], Nucl. Phys. B **689**, 175 (2004)
- [11] D. B. Leinweber, A. W. Thomas, K. Tsushima and S. V. Wright, Phys. Rev. D **64**, 094502 (2001)
- [12] R. D. Young, D. B. Leinweber, A. W. Thomas and S. V. Wright, Phys. Rev. D **66**, 094507 (2002)
- [13] R. D. Young, D. B. Leinweber and A. W. Thomas, Phys. Rev. D **71**, 014001 (2005)
- [14] S. R. Beane, Phys. Rev. D **70**, 034507 (2004)
- [15] S. R. Beane and M. J. Savage, Phys. Rev. D **70**, 074029 (2004) [arXiv:hep-ph/0404131].
- [16] D. B. Leinweber *et al.*, to appear in Phys. Rev. Lett., arXiv:hep-lat/0406002.
- [17] B. Borasoy and R. Lewis, Phys. Rev. D **71**, 014033 (2005) [arXiv:hep-lat/0410042].
- [18] M. Luscher, S. Sint, R. Sommer, P. Weisz and U. Wolff, Nucl. Phys. B **491**, 323 (1997)
- [19] R. G. Edwards, U. M. Heller and T. R. Klassen, Phys. Rev. Lett. **80**, 3448 (1998)
- [20] S. J. Dong, F. X. Lee, K. F. Liu and J. B. Zhang, Phys. Rev. Lett. **85**, 5051 (2000)
- [21] J. M. Zanotti, B. Lasscock, D. B. Leinweber and A. G. Williams, Phys. Rev. D **71**, 034510 (2005)
- [22] G. Rupak and N. Shores, Phys. Rev. D **66**, 054503 (2002) [arXiv:hep-lat/0201019].
- [23] O. Bär, G. Rupak and N. Shores, Phys. Rev. D **70**, 034508 (2004) [arXiv:hep-lat/0306021].
- [24] S. Aoki, Phys. Rev. D **68**, 054508 (2003)
- [25] S. R. Beane and M. J. Savage, Phys. Rev. D **68**, 114502 (2003) [arXiv:hep-lat/0306036].
- [26] S. R. Sharpe and N. Shores, Phys. Rev. D **62**, 094503 (2000) [arXiv:hep-lat/0006017].
- [27] W. Armour *et al.*, in preparation.
- [28] C. K. Chow and S. J. Rey, Nucl. Phys. B **528**, 303 (1998) [arXiv:hep-ph/9708432].
- [29] M. Lublinsky, Phys. Rev. D **55**, 249 (1997)
- [30] R. Sommer, Nucl. Phys. B **411**, 839 (1994) [arXiv:hep-lat/9310022]. R. G. Edwards, U. M. Heller and T. R. Klassen, Nucl. Phys. B **517**, 377 (1998)
- [31] This is two-flavour QCD with the  $q\bar{q}$  force normalised to the physical value at a length scale  $r_0 = 0.49$  fm.

---

[1] Y. Aoki *et al.*, arXiv:hep-lat/0411006.